Misan Journal of Engineering Sciences ISSN: 2957-4242
Vol. 3, No. 2, Dec 2024 ISSN-E: 2957-4250

A Robust Well- Balanced Finite Volume Scheme for the One-Dimensional Shallow Water Equations

Ali Abduljabbar Yousif [1*], Jowhar Rasheed Mohammed[2]

[1,2] *Water Resources Engineering Department, College of Engineering, University of Duhok*
**Corresponding author E-mail: ali.yousif@uod.ac*

(Received 12 Sep, Revised 1 Oct, Accepted 2 Oct)

Abstract: The aim of this study was building a finite volume approach for numerically solving one-dimensional shallow water equations, which applies to flat and non-flat terrain. The devised approach exhibits simplicity and accuracy throughout the time integration process. The proposed methodology used a widely recognized Harten-Lax-Leer (HLL) solver for flux calculation. The suggested finite volume technique is a well-balanced, conservative, non-oscillatory approach ideal for computing the flow depth in various flow regimes of shallow water equations. The developed finite volume model dealt with the steady state of still water in a lake at rest. In addition, the model was validated by applying it to several benchmark tests. The results showed a high concurrence with analytical solutions based on the statistical tests. For the subcritical condition, the standard deviation was 5.73E-03, the root mean square error was 5.84E-03, and the coefficient of determination was 0.9994. For the supercritical condition, the standard deviation was 3.3E-02, the root mean square error was 3.334E-02, and the coefficient of determination was 0.998. Furthermore, the suggested model effectively simulates the Hishkaro River's flow during the flood season.

Keywords: Shallow water equations; Finite volume method; Riemann Solver; HLL; River flow

1. Introduction

In 1871, de Saint-Venant introduced depth-averaged equations that describe the fluid flow. These equations regulate various physical processes. They can model fluid movement in either air or water. Examples include open channel flow, rivers, tsunamis, and flood modeling. Therefore, the equations are highly fascinating to engineers in a variety of applications. Nevertheless, these equations are complex and have required careful attention in applying to special cases to create effective solution techniques [1–5].

The shallow water equations allow for extremely complex flow that may include rarefication and shocks, as well as contact discontinuities in the case of an abrupt change in bottom topography. In engineering applications, the absence of an analytical solution to the shallow water equations is not available for a variety of flow types [6], thus the numerical solution is the best alternative for solving the shallow water equations. There are many difficulties in modeling shallow water equations. The difficulties arise due to the system's dependency on conservation laws; thus, the numerical methods need to maintain a subtle equilibrium between the source terms and flux [7]. This implies that the scheme must accurately maintain the original data corresponding to steady-state solutions that are physically meaningful. The aforementioned schemes are often referred to as well-balanced, and their superiority over other schemes becomes apparent when a coarse computational grid is used to represent solutions that are either steady-state or quasi-steady-state. In such cases, the non-well-balanced scheme's truncation error can exceed the waves to be caught, especially for minor perturbations of steady-state solutions [8]. In addition, a good numerical model for the system of shallow water equations must be able to preserve the positivity of water depths at all-time steps [1,9].

DOI: https://doi.org/10.61263/mjes.v3i2.106

There are several numerical techniques available for solving these equations. These techniques include the differential and integral forms of the shallow water equations. The differential form, which is the basis of finite difference methods, suffers in dealing with discontinuities in the flow since differential equations assume smooth solutions [10]. In contrast, the integral form of the equations is the base of a finite volume approach. Integral equations make no assumptions about the smoothness of their solutions; hence, finite volume techniques can resolve both smooth and non-smooth solutions [11]. However, the accuracy of such numerical approaches will be determined by their integration over time and space [12].

Recently, high-resolution numerical schemes have been presented to deal with different flow phenomena, such as subcritical and supercritical flow [14]. An essential notion in this context is upwind discretization, which is key to this group of approaches. When it comes to high-resolution techniques, the foundation is frequently comprised of mathematical theories that have been demonstrated to be effective for solving one-dimensional homogeneous nonlinear problems. In this context, with the high-resolution schemes, special attention needs to be paid to the treatment of source terms [9]. Additional numerical errors may result from the model's inability to account for high bottom slopes, significant roughness coefficients, and large variability within uneven topography. Therefore, the fluxes and source terms must be discretized in the same manner.

In this paper, a FORTRAN code is built to solve the 1D shallow water equations numerically using finite volume method. The proposed model is then applied to different flow cases to check out the applicability and stability of the simulation model of the flow condition in different flow regimes.

This paper was organized as follows: Section 2, presents the shallow water equations. Section 3 illustrates the finite volume numerical scheme. Section 4 presents the numerical stability. Section 5, presents the results and discussion; and Section 6, illustrates the conclusions drawn from the findings of the study.

2. Governing equations

One common method for simulating river flows is with one-dimensional shallow water equations. Here is a way to express the shallow water equations in one dimension using the hyperbolic conservative form:

$$\frac{\partial \mathrm{U}}{\partial \mathrm{t}} + \frac{\partial \mathrm{F}}{\partial \mathrm{x}} = \mathrm{S} \qquad (1)$$

Where $\mathbf{U}$ represents the conservative variables; $\mathbf{F}$ represents the flux in the direction of flow; and $\mathbf{S}$ is the source terms, which can be written as follows:

$$S = S_0 + S_f \qquad (2)$$

Where $\mathbf{S_0}$ and $\boldsymbol{S_f}$ represent the source terms of bed and friction.

By incorporating source term components into equation (2) and analyzing the bed and friction source terms, we can express the vector terms of the 1D-shallow water equations as follows:

$$U = \begin{bmatrix} h \\ uh \end{bmatrix}, \ F = \begin{bmatrix} uh \\ \frac{(uh)^2}{h} + \frac{1}{2} g h^2 \end{bmatrix}, \ S = \begin{bmatrix} 0 \\ -gh \ S_0 \end{bmatrix} \qquad (3)$$

In this context, h stands for the flow depth, u for the velocity component of the flow direction, uh for the discharges per unit width, and g for the acceleration due to gravity.

It is possible to express the slope of the bed in the x direction as follows:

$$S_0 = -\frac{\partial z}{\partial x} \qquad (4)$$

Where z is the elevation of the bed.

Assuming a rectangular channel and adopting Manning's equation, the friction slope can be expressed in the x-direction as follows [13]:

$$S_f = \frac{n^2 u^2}{h^{4/3}} \qquad (5)$$

Where n stands for the Manning roughness coefficient.

3. Numerical scheme

3.1 Finite volume scheme

The one-dimensional shallow water equations can be expressed in a captivating integral form as follows:

$$\frac{\partial}{\partial t}\int_{\Omega} U \;d\Omega + \int_{S} F \cdot dS + \int_{\Omega} S(x,t)d\Omega = 0 \tag{6}$$

Figure (1) below shows the typical domain of a one-dimensional solution.

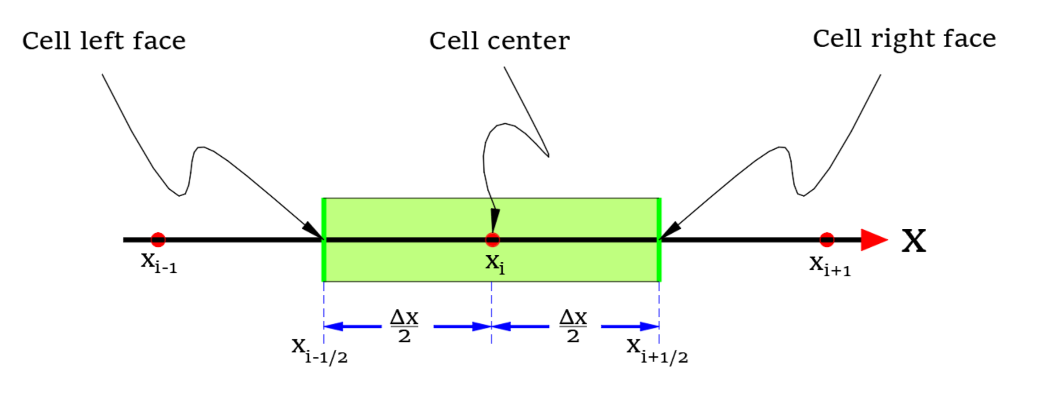

Figure 1. Typical cell properties of a one-dimensional domain in a finite volume.

Finding a solution to the conservation law is the finite volume aim, which leads to the following discrete description of the conservation law system:

$$\frac{U_i^{n+1}-U_i^n}{\Delta t} + \frac{F_{i+1/2}^n - F_{i-1/2}^n}{\Delta x} - \frac{S^n_{i+\frac{1}{2}} + S^n_{i-\frac{1}{2}}}{2} = 0 \tag{7}$$

Figure (1) above shows that the discrete U-values are the averages of the conservative variables inside each given cell (i); this method is explicit since it evaluates fluxes and source terms at the cell interfaces and at time level n. The conservative variables in equation 8 may be expressed as follows, using the upwind technique for both the flow and source terms:

$$U_i^{n+1} = U_i^n + \frac{\Delta t}{\Delta x}\left(F^n_{i+\frac{1}{2}} - F^n_{i-\frac{1}{2}}\right) = \frac{\Delta t}{2}\left(S^n_{i+\frac{1}{2}} + S^n_{i-\frac{1}{2}}\right) \tag{8}$$

3.2 The HLL flux solver:

The cell interface of the Riemann problem is considered here as follows:

$$U(x,0) = \begin{cases} U_j & if \quad x < 0 \\ U_{j+1} & if \quad x > 0 \end{cases} \tag{9}$$

Originally, Harten et al., 1983 suggested a single state between the left and right states as follows:

$$\tilde{U}\left(\frac{x}{t}\right) = \begin{cases} U_j & if \quad x < S_L t, \\ U^{HLL}_{j+\frac{1}{2}} & if \quad S_L t < x < S_R t \\ U_{j+1} & if \quad x > S_R t \end{cases} \tag{10}$$

Where S_L *and* S_R are the approximations of the smallest and largest wave velocities at the interface $X_{J+1/2}$, respectively. Figure (2) shows the HLL approximate Riemann solver.

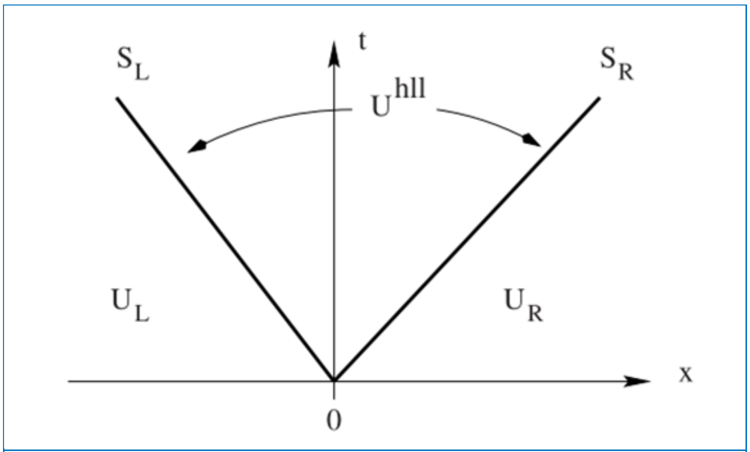

Figure 2. Approximate HLL Riemann solver (Toro, 2009).

The $\mathbf{U}^{\mathrm{HLL}}_{j+1/2}$ is the intermediate state that can be introduced to keep the Riemann solver reliable with the conservation law's integral form, as follows:

$$U^{HLL}_{j+1/2} = \frac{S_R U_{j+1} - S_L U_j + F_j - F_{j+1}}{S_R - S_L} \tag{11}$$

Then, the flux function $\mathbf{F}_{j+1/2}$ can be determined using the $\mathbf{U}^{\mathrm{HLL}}_{j+1/2}$ as following:

$$F_{j+1/2} = \begin{cases} F_j & if \quad 0 < S_L \\ F^{HLL}_{j+1/2} & if \quad S_L < 0 < S_R \\ F_{j+1} & if \quad 0 > S_R \end{cases} \tag{12}$$

To derive the flux function for the non-trivial subsonic case $S_{\mathrm{L}} < 0 < S_{\mathrm{R}}$, the following form is used:

$$\begin{aligned} F^{HLL}_{j+1/2} &= F_j + S_L\left(U^{HLL}_{j+1/2} - U_j\right) \\ F^{HLL}_{j+1/2} &= F_{j+1} + S_R\left(U^{HLL}_{j+1/2} - U_{j+1}\right) \end{aligned} \tag{13}$$

The forms in equation (13) are equivalent, so incorporating any of them with equation (11) results:

$$F^{HLL}_{j+1/2} = \frac{S_R F_j - S_L F_{j+1} + S_L S_R (U_{j+1} - U_j)}{S_R - S_L} \tag{14}$$

Now, incorporating equations 12 and 14 results in the flux of HLL as follows:

$$F_{j+1/2} = \frac{S_R F_j - S_L F_{j+1} + S_L S_R (U_{j+1} - U_j)}{S_R - S_L} \tag{15}$$

Now, the HLL intercell flux can be determined using

$$F^{HLL}_{j+\frac{1}{2}} = \begin{cases} F_L & if\, 0 \le S_L, \\ \frac{S_R F_L - S_L F_R + S_L S_R (U_R - U_L)}{S_R - S_L}, & if\, S_L \le 0 \le S_R \\ F_R & if\, 0 \ge S_R. \end{cases} \tag{16}$$

4. Numerical Stability:

Through the utilization of the Courant-Friedrichs-Lewy (CFL) condition, which was initially presented by Courant et al. [15], it is possible to fulfill the stability criteria for an explicit one-dimensional numerical simulation. The time step is found by using the following formula:

$$\Delta t = CFL \cdot \min_i \left(\frac{\Delta x}{|\lambda|_i^n}\right) \quad \dots . CFL < 1 \tag{17}$$

In this context, Δt denotes the time step, CFL stands for the Courant-Friedrichs-Lewy number, Δx is the cell size in 1D, and λ is the celerity speed of the flow.

5. Numerical results:

5.1 Lake at rest test:

This test is typically conducted to check whether the finite volume scheme can model the still-water steady-state condition. Following the researcher [10], the length of the lake is considered at 1500 m, and the downstream boundary condition to 12 m. The initial condition is also assumed to be 12 m. The geometry of the lake's bed profile is given in Table (1). Figure (3) shows the results of the water surface elevation for a 10-second simulation and the domain was discretized every 5 m. It can be seen that the developed model is well-balanced, which means that the steady-state condition for the lake at rest is maintained up to a discrete level.

Table 1. Bathymetry of the lake's bed.

x (m)	0	50	100	150	250	300	350	400	425	435	450	470	475	500	505
z (m)	0	0	2.5	5	5	3	5	5	7.5	8	9	9	9	9.1	9
x (m)	530	550	565	575	600	650	700	750	800	820	900	950	1000	1500	
z (m)	9	6	5.5	5.5	5	4	3	3	2.3	2	1.2	0.4	0	0	

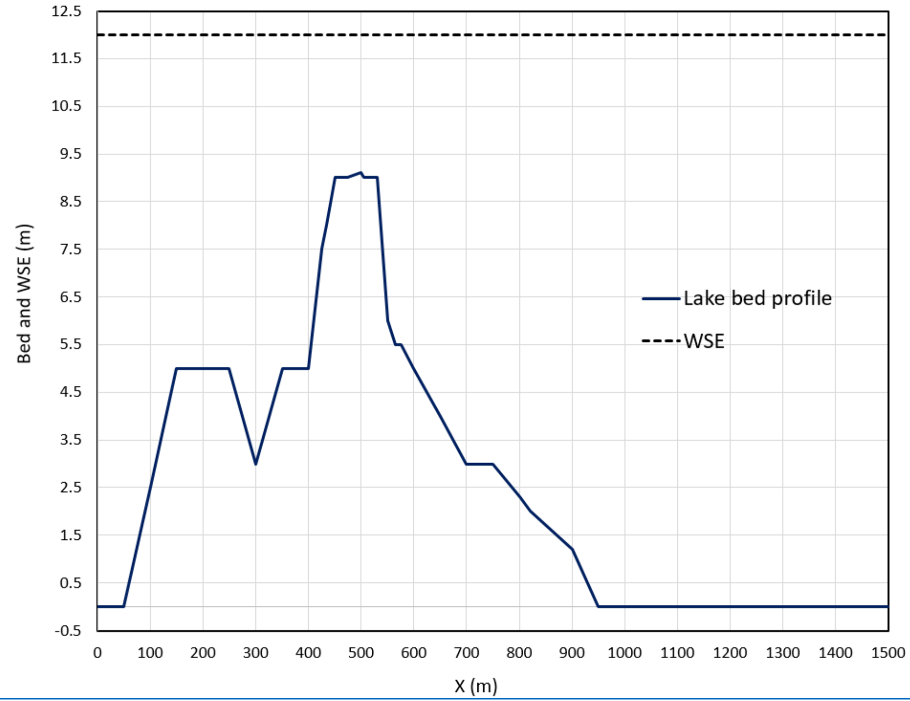

Figure 3. Water surface elevation.

5.2 Steady state flow over a hump

The developed model is validated against benchmark tests described in [7]. These tests have been used in many other literature such as [16] and [17]. The steady-state conditions were imposed by using two different combinations on a frictionless and flat rectangular channel. The channel length is 25 m, and the width is a unit. The channel bed elevation changes due to the bump. The bump elevation is given as the following:

$$Z(x) = \begin{cases} 0.8 * (1 - \frac{(X-10)^2}{4}) & if 8 \leqslant x \leqslant 12 \\ 0 & otherwise \end{cases} \quad (18)$$

To secure the robustness of the developed scheme and to see how the model behaves against different flow regimes, two different flow conditions were used and described in Table (2).

Table 2. Flow conditions for the test cases (boundary conditions).

Test	Upstream BC (m^2/sec)	Downstream BC (m)
A	q= 1	h=1.7
B	q= 0.4	Transmissive

Test A describes a non-transitional fully subcritical flow, whereas test B describes the robustness of the model against upstream subcritical flow and downstream supercritical flow.

The Bernoulli principle, also known as head conservation, was utilized to compute the analytical solutions for tests A and B [4]. The analytical solution was computed using the concept of energy conservation for a rectangular channel, given as follows:

$$E_i = \eta_{i+1} + \frac{1}{2g}\frac{q_{x,i}^2}{h_{x,i}^2} \quad (19)$$

Figures (4) and (5) show a graphical demonstration of the comparison between the analytical values and the numerical findings that were achieved by our model. What appears to be the case is that the newly developed algorithm generates results that are compatible with the analytical solution. Nevertheless, there is a slight disparity in water depth that can be observed between the analytical solution and the numerical results. Thus, to quantify the differences that exist between the analytical solution and the numerical solution, three statistical tests were carried out, namely the standard deviation, the root mean square error, and the coefficient of determination. The standard deviation was computed as follows:

$$\sigma(E) = \sqrt{\frac{\sum(diff(h)-\mu(E))^2}{N}} \quad (20)$$

Where, $\sigma(E)$ is the standard deviation of the error (E) between the numerical and analytical depth, $\mu(E)$ is the mean of error in h between numerical and analytical depths and N is the total number of cells. The root mean square error was computed as follows:

$$RMSE = \sqrt{\frac{\sum(E)^2}{N}} \quad (21)$$

The coefficient of determination was computed as follows:

$$R^2 = \left[\frac{n(\sum h_n h_a)-(\sum h_n)(\sum h_a)}{[n\sum h_n{}^2-(\sum h_n)^2][n\sum h_a{}^2-(\sum h_a)^2]}\right]^2 \quad (22)$$

Where, h_n is the numerical water depth and h_a is the analytical water depth.

The statistical analysis showed that, for the subcritical flow test case, the standard deviation in the error was 5.73E-03, the RMSE was 5.84E-03, and the coefficient of determination between the numerical depth and analytical depth was 0.9994. Whereas, for the supercritical test case, the standard deviation was 3.3E-02, the RMSE was 3.33E-02, and the coefficient of determination was 0.998. For both test cases, the proposed model behaves very well based on the standard deviation of the error and the root mean square error results as they are very small. In addition, the coefficient of determination for both test cases was very high, which showed that the numerical depth is behaving in similar way of analytical depth.

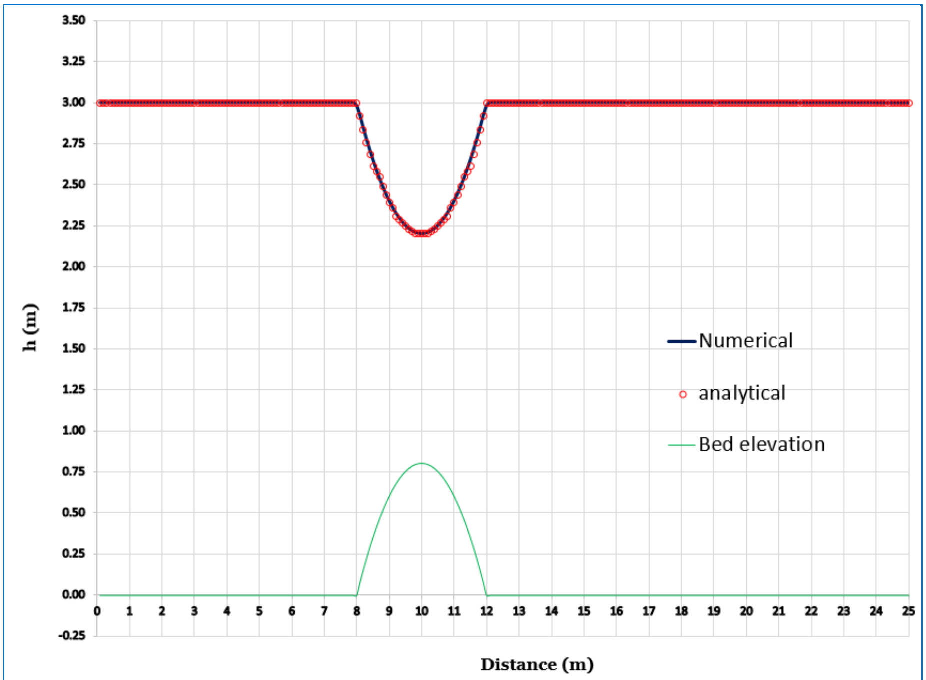

Figure 4. Numerical and analytical water depth for subcritical condition (test A).

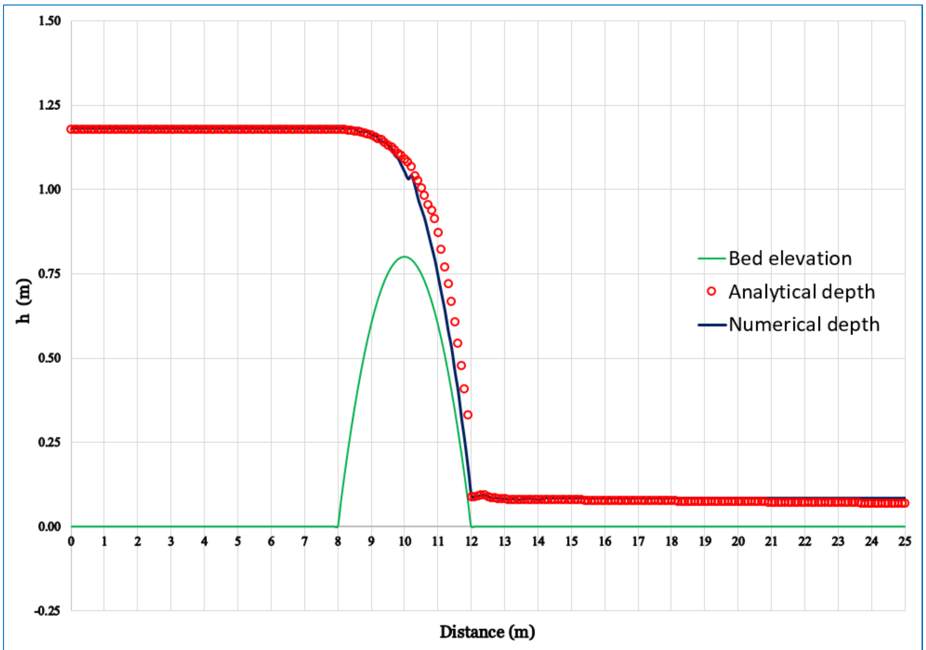

Figure 5. Numerical and analytical water depth for supercritical condition (test B).

5.3 Application of the model to Hishkaro river

The proposed model in this study is applied to the Hishkaro River. The full description of the Hishkaro basin is given in [18]. To determine the discharge in the river during flood events, the basin is divided into two parts, to the left and right of the river, following the flow direction in the main river section. The two parts are separated using the original mesh which was used for the 2D mesh process given in [18]. Figure (6 A) shows the topography of part 1 (the right side) of the Hishkaro basin. The total area of this part is 19.7225 Km^2. This part consists of 22992 nodes, which generate 45269 triangular cells. The minimum triangle length was 15.394 m and the maximum triangle length was 494.77 m. Figure (6 B) shows the topography of part 2 (the left side) of the basin.

The total area of part 2 is 22.301 Km^2. This part consists of 25411 nodes which produce 49898 triangular cells. The minimum triangle length was 17.08 m, and the maximum triangle length was 94.868 m.

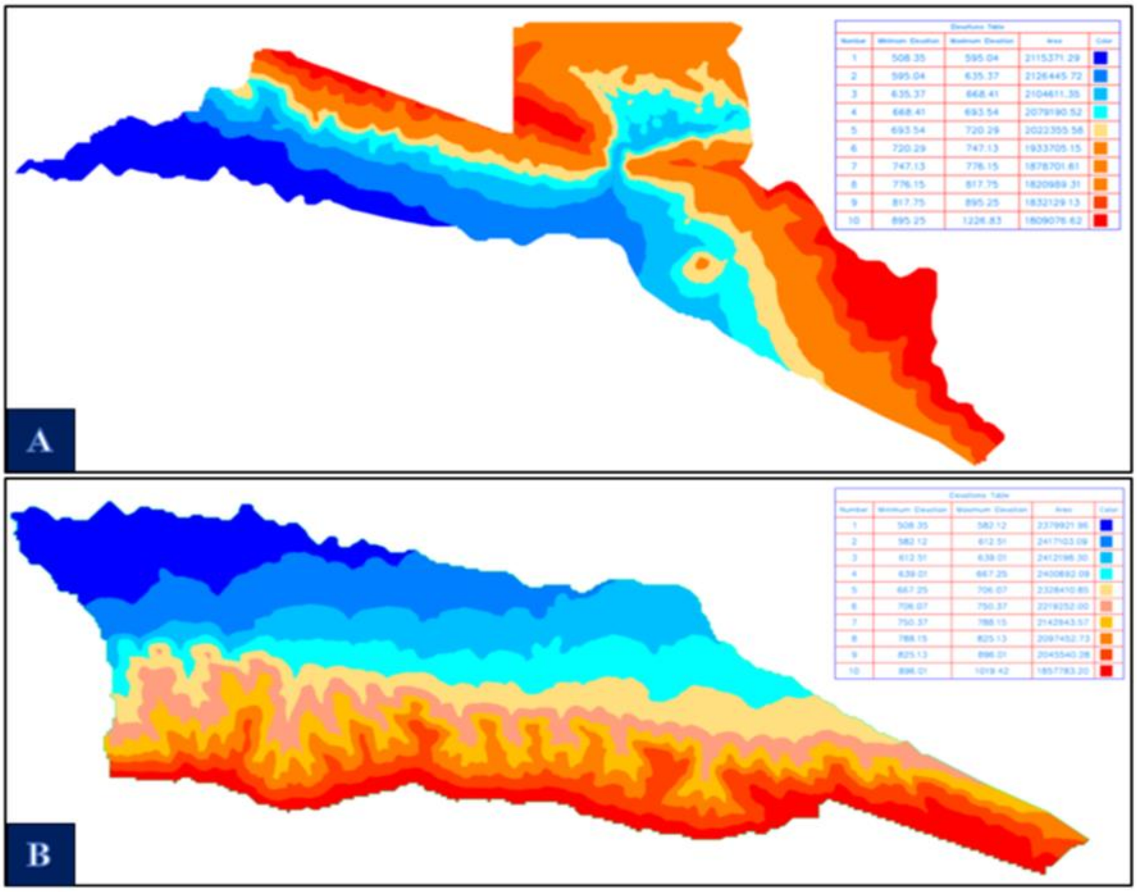

Figure 6. Topography of the Hishkaro basin sides: right bank (A) and left bank (B).

Figure (7) shows the longitudinal profile of the river. The length of the river is 14.98 km. The maximum upstream elevation of the river is 814.3 m, and the minimum elevation is 507.223 m at the outlet of the river.

In this study, the 1D river domain is divided into 500 nodes, which creates 499 1D cells. Each 1D cell is connected to two 2D cells, one from the left side and another from the right side. Thus, the lateral flow that enters each 1D cell is the accumulation of the flows from the adjacent 2D cells over the time step.

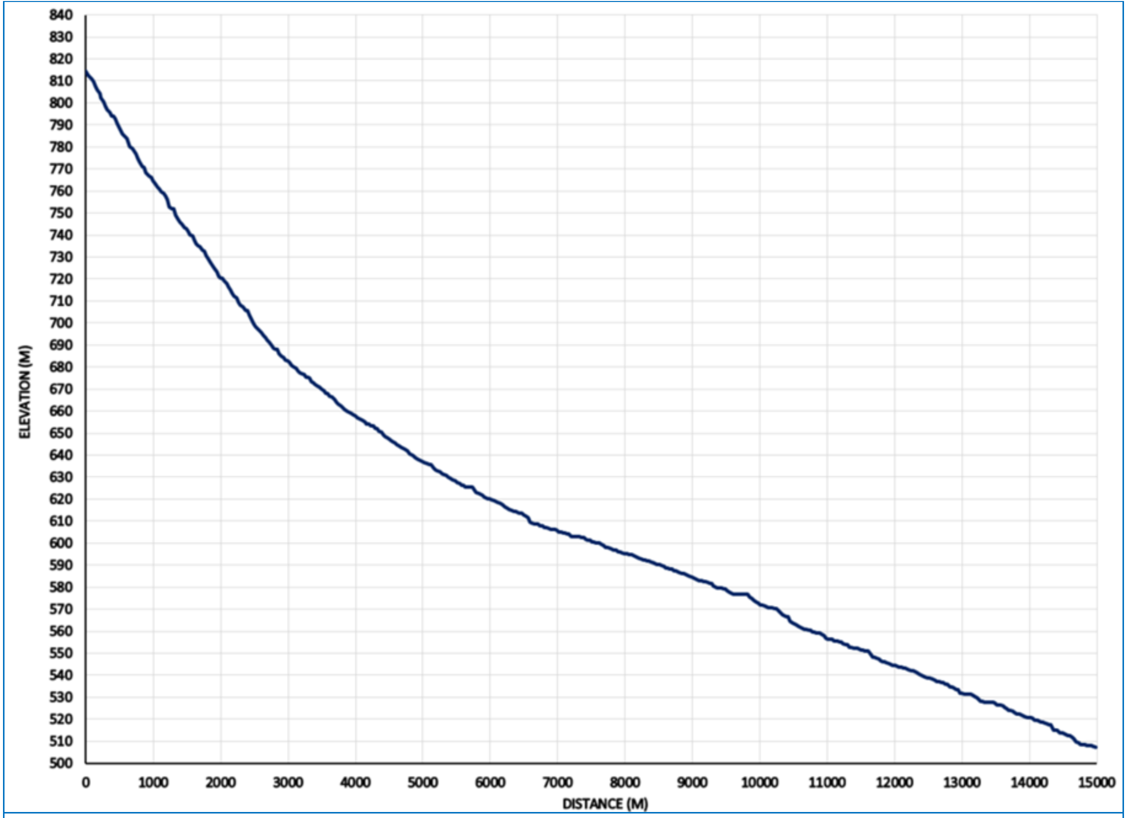

Figure 7. Longitudinal profile of the river path.

The proposed model in this study is applied to determine the hydrograph of flow at the outlet of the basin due to the flood event of 35 mm/hr for 1 hour over the Hishkaro catchment. The time step for this simulation was 0.6 seconds, which is the same as the time step for the 2D model given in [18], since it is usually much smaller than the required time step for the 1D model. Figure (8) shows the resulting hydrograph for the suggested 20 m river width at the outlet point. From Figure (8) it can be seen clearly that the maximum discharge occurs at 204 minutes from the beginning of the rainfall, where the discharge reaches 133.97 m^3/sec. In addition, it is obvious from the figure that the time between 195 minutes and 208 minutes is critical, where at this period the discharge is always above 100 m^3/sec.

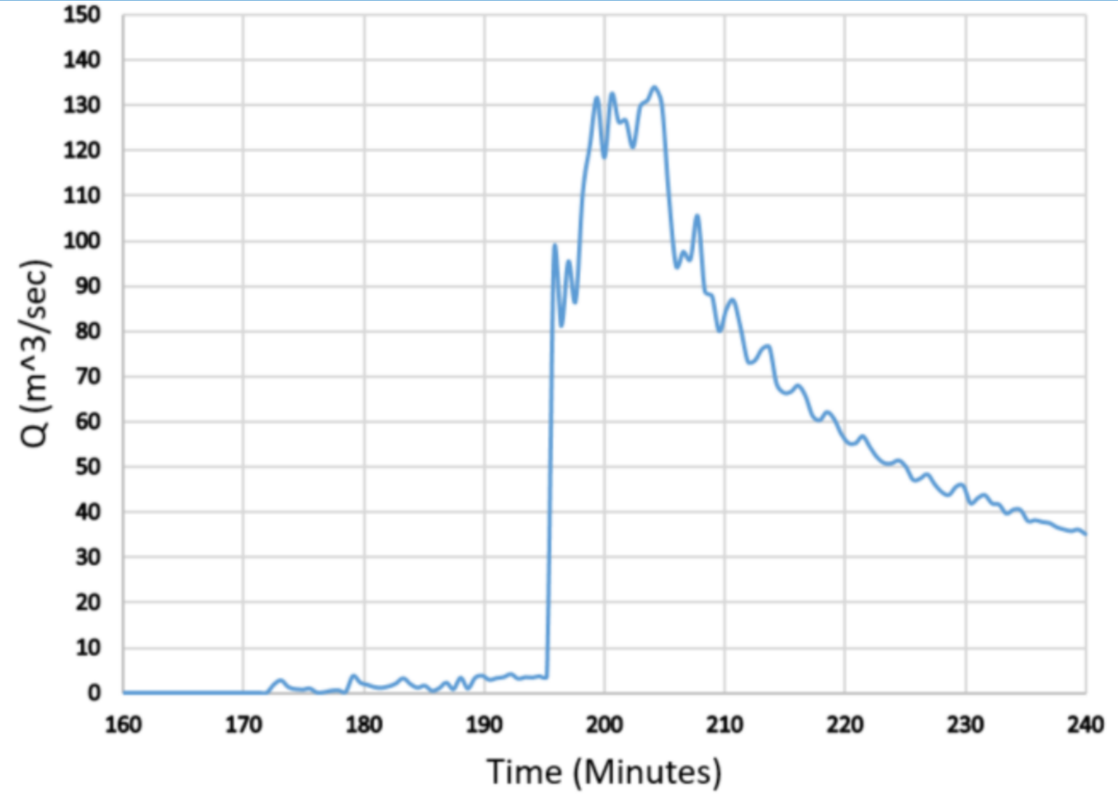

Figure 8. Hydrograph at the outlet for a rainfall intensity of 35 mm/hr.

6. Conclusions

In this paper, a robust and well-balanced 1D finite volume scheme with an HLL solver was developed. It is well known that even in the absence of physical energy loss, numerical changes in energy are induced by solving the discrete equation of momentum conservation, even for flows in frictionless channels. However, the developed model was able to predict the flow depths over the domain very well with very small errors. From the analysis of test cases and application of the model to the Hishkaro River, the following conclusions can be drawn:

1- The developed model in this study showed its robustness to deal with the steady state of still water when it passed the lake at rest test.
2- The developed model in this study is able to simulate different flow conditions in open channels such as subcritical flow and upstream subcritical and downstream supercritical flow. This is based on the results of the standard deviation, the root mean square error for the errors between the numerical and analytical analysis, and the coefficient of determination. For the subcritical test case, the standard deviation, the root mean square, and the coefficient of determination were 5.73E-03, 5.84E-03, and 0.9994, respectively. Whereas, the same statistical analysis for the supercritical test case were 3.3E-02, 3.334E-02, and 0.998, respectively.
3- The proposed model was successfully able to simulate the flow in the Hishkaro River during the flood period.

Acknowledgments

The authors would like to express their sincere gratitude to the College of Engineering at the University of Duhok for their valuable support in conducting this research. Their resources, guidance, and encouragement played a crucial role in the successful completion of this study.

Author Contributions: The authors contributed to all parts of the current study.

Funding: This study received no external funding.

Conflicts of Interest: The authors declare no conflict of interest.

References

[1] Murillo J, García-Navarro P. Accurate numerical modeling of 1D flow in channels with arbitrary shape. Application of the energy balanced property. Journal of Computational Physics 2014; 260: 222–248. DOI: 10.1016/j.jcp.2013.12.040.

[2] Toro EF. Riemann solvers and numerical methods for fluid dynamics: A practical introduction 2009; doi:10.1007/b79761.

[3] Franzini F, Soares-Frazão S. Efficiency and accuracy of Lateralized HLL, HLLS and Augmented Roe's scheme with energy balance for river flows in irregular channels. Applied Mathematical Modelling 2016; 40(17–18): 7427–7446. DOI: 10.1016/j.apm.2016.02.007.

[4] Bruwier M, Archambeau P, Erpicum S, Pirotton M, Dewals B. Discretization of the divergen -ce formulation of the bed slope term in the shallow-water equations and consequences in te rms of energy balance. Applied Mathematical Modelling 2016; 40(17–18): 7532–7544. DOI: 10.1016/j.apm.2016.01.041.

[5] Gouta N, Maurel F. A finite volume solver for 1D shallow-water equations applied to an actual river. International Journal for Numerical Methods in Fluids 2002; 38(1): 1–19. DOI: 10.1002/fld.201.

[6] Kurganov A. Finite-volume schemes for shallow-water equations. Acta Numerica 2018; 27 (May): 289–351. DOI: 10.1017/S0962492918000028.

[7] Aureli F, Maranzoni A, Mignosa P, Ziveri C. A weighted surface-depth gradient method for the numerical integration of the 2D shallow water equations with topography. Advances in Water Resources 2008; 31(7): 962–974. DOI: https://doi.org/10.1016/j.advwatres.2008.03.005.

[8] Navas-Montilla A, Murillo J. Overcoming numerical shockwave anomalies using energy balanced numerical schemes. Application to the Shallow Water Equations with discontinuous t opography. Journal of Computational Physics 2017; 340: 575–616. DOI: 10.1016/j.jcp.2017.03. 057.

[9] García-Navarro P, Brufau P, Burguete J, Murillo J. The shallow water equations: An example of hyperbolic system. Monografías de La Real Academia de Cienciasde Zaragoza 2008; 31: 89–119.

[10] Hidayat N, Suhariningsih, Suryanto A, Mungkasi S. The significance of spatial reconstructio n in finite volume methods for the shallow water equations. Applied Mathematical Sciences 2014; 8(29–32): 1411–1420. DOI: 10.12988/ams.2014.4124

[11] Kurganov A, Noelle S, Petrova G. Semi-discrete central-upwind schemes for hyperbolic cons ervation laws and Hamilton-Jacobi equations. 2002; doi:10.1137/S1064827500373413.

[12] LeVeque RJ. Finite-volume methods for hyperbolic problems. 2004; www.cambridge.org/0521 810876.

[13] Chow V. Te. Open channel hydraulics. 1959; New York, McGraw-Hill, 680 p.

[14] Harten A, Lax PD, Leer B van. On Upstream Differencing and Godunov-Type Schemes for Hyperbolic Conservation Laws. SIAM Review 1983; 25(1): 35–61. DOI: 10.1137/1025 002.

[15] Courant R, Friedrichs K, Lewy H. On the Partial Difference Equations of Mathematical Physics. IBM Journal of Research and Development 1967; 11(2): 215–234. DOI: 10.1147/rd. 112.0215.

[16] Lundgren L. Efficient numerical methods for the shallow water equations. 2018; M. Sc. Thesis. Faculty of science and technology, UPPSALA University.

[17] Goffin L, Dewals B, Erpicum S, Pirotton M, Archambeau P. An Optimized and Scalable Algorithm for the Fast Convergence of Steady 1-D Open-Channel Flows.Journal of Water 20 20; 117–125.

[18] Yousif AA, Mohammed JR. A robust unstructured finite volume scheme for urban flash flood simulation: Duhok city as a case study. ISH Journal of Hydraulic Engineering 2024; 3 0(2): 245–253. DOI: 10.1080/09715010.2023.2293986.